Join our webinar to learn how

Image Credit: Stockdevil/iStockphoto

Less is more: Using microCT to assess bone loss in preclinical models

Webinar Details:
September 29, 2017
8:00 AM PDT
11:00 AM EDT
5:00 PM CEST

Register Here

PerkinElmer® *For the Better*

CURRENT PROTOCOLS
A Wiley Brand

WILEY

307902

Analysis of Cell Growth and Diffusion in a Scaffold for Cartilage Tissue Engineering

C.A. Chung, C.W. Yang, C.W. Chen

Department of Mechanical Engineering, National Central University, Jhongli, Taiwan 320, R.O.C.; telephone: +886 3 4267333; fax: +886 3 4254501; e-mail: cachung@ncu.edu.tw

Received 18 November 2005; accepted 13 March 2006

Published online 3 April 2006 in Wiley InterScience (www.interscience.wiley.com). DOI: 10.1002/bit.20944

Abstract: Developments in tissue engineering over the past decade have offered promising future for the repair and reconstruction of damaged tissues. To regenerate three dimensional and weight-bearing implants, advances in biomaterials and manufacturing technologies prompted cell cultivations with natural or artificial scaffolds, in which cells are allowed to proliferate, migrate, and differentiate in vitro. In this article, we develop a mathematical model for cell growth in a porous scaffold. By treating the cell-scaffold construct as a porous medium, a continuum model is set up based on basic principles of mass conservation. In addition to cell growth kinetics, we incorporate cell diffusion in the model to describe the effects of cell random walks. Computational results are compared to experimental data found in the literature. With this model, we are able to investigate cell motility, heterogeneous cell distributions, and non-uniform seeding for tissue engineering applications. Results show that random walks tend to enhance uniform cell spreads in space, which in turn increases the probabilities for cells to acquire nutrients; therefore random walks are likely to be a positive contribution to the overall cell growth on scaffolds. © 2006 Wiley Periodicals, Inc.

Keywords: tissue engineering; cell culture; mass transfer; cell migration; random walk

INTRODUCTION

Tissues engineering is an inter-discipline that applies knowledge of life science and engineering to the development of biological substitutes that can be used to maintain or repair damaged tissues (Langer and Vacanti, 1993). The engineered tissues may offer the potential to reduce or remove the needs for organ transplants. Three principal therapeutic strategies that have been proposed to treat wounded tissue in patients are (i) implantation of dissociated cells; (ii) implantation of biodegradable scaffolds along to stimulate in situ tissue regeneration; (iii) implantation of generated tissues from in vitro cell-scaffold constructs (Griffith and Naughton, 2002). As compared to the first two strategies, the usage of cell-scaffold constructs improves the location of cell delivery and promotes graft fixation and survival. Therefore, cultivation of cells on scaffolds has been drawing great research efforts. A variety of materials that have been reported for the manufacturing of scaffolds include natural materials such as collagen, glycosaminoglycan, and chitosan. In addition to natural materials, artificially synthetic polymers like polyglycolic acid (PGA), polylactic acid (PLA), and polycaprolactone (PCL) have also been tested (Pachence and Kohn, 2000). Biomaterials are believed to play an important role in the development of engineered tissues. Physicochemical interactions between cells and the solid matrices have to be carefully considered. It is now accepted that a biomaterial must interact with tissues to repair rather than only act as a passive, supporting structure (Peppas and Langer, 1994).

Fabrications of cell-scaffold constructs of clinically relevant dimensions and filled with neo cells of proper phenotypes still pose a challenge. In the context of articular cartilage engineering, a wide range of experimental studies have been conducted to investigate in vitro chondrogenesis (Freed et al., 1994a,b; Malda et al., 2005; Obradovic et al., 1999). Dimensions of the scaffolds have not yet gone beyond hundreds of micrometers. This difficulty has been attributed to diffusion limits of the nutrients like glucose and oxygen, and metabolites throughout the cell-scaffold composites, which could hinder cell growth in the scaffold. Such a problem might be solved by developing adequate scaffolds with large enough porosity and/or by enhancing chemicals transport with suitable hydrodynamic bioreactors (Obradovic et al., 1999; Pazzano et al., 2000). Meanwhile, a series of mathematical models were being developed to quantify relevant parameters for cell growth within scaffolds. Freed et al. (1994a) developed an empirical equation for the analysis of cell culture in a PGA scaffold. Later on, models that measured cell density distribution and oxygen concentration were also been set up (Lewis et al., 2005; Obradovic et al., 2000). More recently, researchers were devoted to the development of more sophisticated mathematic models, considering cell-scaffold constructs a porous medium and using a volume average method, to elucidate the distribution of glucose concentration and its corresponding effect on cell number density (Galban and Locke, 1999a,b). Mathematical

Correspondence to: C.A. Chung
Contract grant sponsor: National Science Council of Taiwan

works that analyzed the interactions between cells and nutrients confirmed the effects of diffusion limits of nutrients over cell viability.

To date, most mathematic models have not yet taken into account cell migration for tissue engineering. Mature chondrocytes are round shaped and believed to be a non-motile cell type. Therefore, the motility of chondrocytes on scaffolds has not been rigorously investigated. However, it was shown that chondrocytes in vitro could be motile in primary culture (Chang et al., 2003; Frenkel et al., 1996). In the experiment of Chang et al., it was found 30% of population moved on a fibronectin-coated membrane with speeds larger than 1 μm/h, and with directional persistence longer than 1 h. Recently, it was also reported that passaged chondrocytes could move in vitro (Hamilton et al., 2005). Since the number of isolated cells from a patient's biopsy is often too small for direct seeding, the combined process of monolayer expansion in Petri dishes for one or two passages and then spatial growth in 3D scaffolds is so far most likely. It is, therefore, possible that neo cells on scaffolds are motile, which should affect the cell distribution and growth to some extent. In this work, we develop a mathematical model, incorporating cell motility due to random walks, to describe the interaction between cell proliferation and nutrient consumption based on a porous medium approach and volume average method. Results of the numerical simulations are compared with experimental data to verify its validity. After that, effects of cell diffusion on non-uniform seeding are analyzed. Finally suggestions for cartilage engineering are drawn in the conclusion according to the investigation of cell migration and its effects on the chondrogenesis.

MODEL FORMULATION

An approach to a cartilage transplant includes a sequence of events. First a small biopsy of cells is taken from the patient. After expansion in monolayer culture, cells are seeded in a scaffold, which is made of either natural materials like collagen, or artificially synthesized polymers such as PGA or PLA. The celled scaffold is then submerged in a culture well filled with culture media for steady culture or put in a dynamic bioreactor that is designed to enhance nutrient transports by perfusion or rotation. Scaffolds must have large enough porosity so that nutrients can be delivered easily to the cells. Porosities have been reported in literatures to be as high as 95% (Freed et al., 1994a). In this work, we focus on the stage of cell culture on a scaffold, considering (i) nutrient transports are only by diffusion in both the cell colony space (σ phase) and the interstitial medium space (β phase); (ii) growth of the cells are due to cell proliferation. The σ phase is considered to comprise both cells and extracellular matrix (ECM). The difference in the mass diffusivity between the cells and ECM is neglected. Nutrients are simplified to be a single species. It is also assumed that porosity of the scaffold is so high that it performs no inhibition against nutrient transports. Therefore, the solid matrix is ignored here, and a biphasic porous medium comprising cell colony space (σ phase) and interstitial fluid (β phase) is assumed.

Mass Conservation of Nutrient

For mammalian cells, glucose is among the principal energy sources (Obradovic et al., 1999). In this work, we assume glucose to be the diffusion-limited nutrient. The species continuity equation for glucose includes diffusive transport in both the cell phase and fluid phase, and consumption in the cell phase. Following the volume average method of Wood et al. (2002), the macro scale conservation equations governing the nutrient concentration can be written as

$$\frac{\partial}{\partial t'}\left[\varepsilon_\beta\langle c_\beta\rangle^\beta+\varepsilon_\sigma\langle c_\sigma\rangle^\sigma\right]=\nabla\cdot\left(\mathbf{D}^\beta_{\text{eff}}\cdot\nabla\langle c_\beta\rangle^\beta+\mathbf{D}^\sigma_{\text{eff}}\cdot\nabla\langle c_\sigma\rangle^\sigma\right)-\hat{R}_{\text{m}}\varepsilon_\sigma\langle c_\sigma\rangle^\sigma \tag{1}$$

In the equation, the volume fractions of the two phases are defined as

$$\varepsilon_\beta=\frac{V_\beta}{V},\quad \varepsilon_\sigma=\frac{V_\sigma}{V} \tag{2a, b}$$

where the volume V represents the elementary volume illustrated in Figure 1 and the phase volumes, V_β and V_σ, are the volumes of the fluid and cell phases within V. The intrinsic average concentrations are defined for nutrients in the fluid and cell phases as

$$\langle c_\beta\rangle^\beta=\frac{1}{V_\beta}\int_{V_\beta(t)}c_\beta\mathrm{d}V \tag{3a}$$

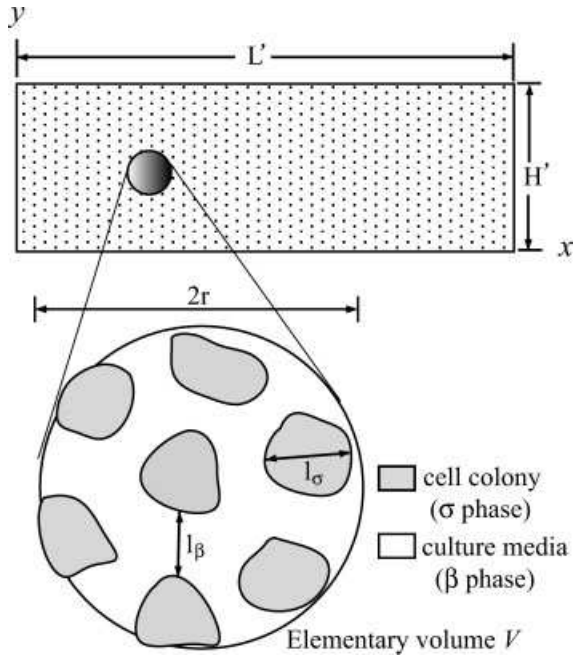

Figure 1. Schematic diagram of the cell-scaffold construct. The enlarged area denotes the elementary volume, which comprises the cell colony and culture medium phases.

$$\langle c_\sigma \rangle^\sigma = \frac{1}{V_\sigma} \int_{V_\sigma(t)} c_\sigma \mathrm{d}V \tag{3b}$$

Equation (1) states that the change rate of nutrient mass in a representative elementary volume is balanced by the diffusion and the nutrient consumption by cellular metabolism. In the diffusion term, coefficients $\mathbf{D}^\beta_{\text{eff}}$ and $\mathbf{D}^\sigma_{\text{eff}}$ represent effective diffusion tensors for nutrients in the fluid and cell phases, respectively. The effective diffusion tensors comprise both the macro and subcellular scale transports (Wood et al., 2002). The length scale constraints required in the method of volume average have been given in detail in previous literature (Carbonell and Whitaker, 1984). The length scales l_β and l_σ of the fluid and cell phases, respectively must be small compared to the radius of the elementary volume. In general, these ideas are expressed as

$$l_\beta, l_\gamma << r << H' \tag{4}$$

where r is the characteristic radius of the elementary volume, and H' can be seen as the thickness of the scaffold as shown in Figure 1. A discussion of the length scales is given by Galban and Locke (1999a): $l_\beta \approx 14$ μm, $l_\sigma \approx 11$ μm, $r \approx 25$ μm, and $H' \approx 0.1$ cm. Therefore, the constraints hold usually. Finally, the chemical reaction is defined through the metabolic rate coefficient $\hat{R}_{\text{m}}$ by assuming that the consumption is proportional to the nutrient concentration.

We further assume that the fluid and cell phases are in equilibrium with respect to the interfacial transport process (Wood et al., 2002), which yields

$$\langle c_\sigma \rangle^\sigma = K_{\text{eq}} \langle c_\beta \rangle^\beta \tag{5}$$

where K_{eq} is the equilibrium coefficient. If the mass transfer across the interface is much faster than diffusion, a local mass equilibrium can be assumed to hold, that is, the macroscale concentrations are tied to each other by an equilibrium relation of the form. By using Equation (5), we can have a single unknown, the nutrient concentration variable in the β phase, governed by the following equation

$$\frac{\partial}{\partial t'}\left[(\varepsilon_\beta + \varepsilon_\sigma K_{\text{eq}})\langle c_\beta \rangle^\beta\right] = \nabla \cdot \left(\hat{\mathbf{D}}_{\text{eff}} \cdot \nabla \langle c_\beta \rangle^\beta\right) - \hat{R}_{\text{m}} K_{\text{eq}} \varepsilon_\sigma \langle c_\beta \rangle^\beta \tag{6}$$

Before Equation (6) can be used to solve $\langle c_\beta \rangle^\beta$, one has to specify the overall effective diffusion tensor that appears in Equation (6). If the subcellular transport is negligible, then the overall effective diffusion tensor is reduced to an isotropic tensor $\hat{\mathbf{D}}_{\text{eff}} = \hat{D}_{\text{eff}}\mathbf{I}$, where the effective diffusivity is simply equal to a weighted arithmetic mean

$$\hat{D}_{\text{eff}} = \varepsilon_\beta D_\beta + \varepsilon_\sigma K_{\text{eq}} D_\sigma \tag{7}$$

Here D_β and D_γ are the molecular diffusion coefficients of the nutrient in the fluid and cell phases, respectively. This simplified equation is valid under the situation that the subcellular transport is negligibly small. If it is not, more sophisticated analytical formula of the overall effective diffusion tensor can be adopted (Chang, 1983; Ochoa et al., 1986). More recently, Wood et al. (2002) developed a numerical scheme for calculating the effective diffusivity for biofilms and tissues.

Mass Conservation of Cells

Cell proliferation and migration are basic to life cycle. Cell distributions in a scaffold can be affected by two factors. The first is the amount of nutrients that can be transported in from the medium surrounding the polymer scaffold. The second is the cell motion. Notwithstanding, mature chondrocytes were considered a non-motile cell type, it was being shown that both primary and passaged chondrocytes might migrate (Chang et al., 2003; Hamilton et al., 2005). In this work, we incorporate cell motility into our model by considering the cell diffusion due to the effect of cell random walks. Following previous studies of modeling bacteria distributions (Britton, 2002; Hillesdon et al., 1995), the volume average equation of cell mass can be written by considering the conservation of cell mass as

$$\frac{\partial}{\partial t'}\left[\varepsilon_\sigma \langle \rho_\sigma \rangle^\sigma\right] = \nabla \cdot \left[D_{\text{cell}} \nabla (\varepsilon_\sigma \langle \rho_\sigma \rangle^\sigma)\right] + \left[\frac{R_{\text{g}} \langle c_\sigma \rangle^\sigma}{K_{\text{c}}(\rho_{\text{cell}} \varepsilon_\sigma) + \langle c_\sigma \rangle^\sigma} - R_{\text{d}}\right] \varepsilon_\sigma \langle \rho_\sigma \rangle^\sigma \tag{8}$$

In the equation, the intrinsic average cell mass density is defined as

$$\langle \rho_\sigma \rangle^\sigma = \frac{1}{V_\sigma} \int_{V_\sigma(t)} \rho_\sigma \mathrm{d}V \tag{9}$$

where the mass density of cell phase, ρ_σ, includes both the cells and ECM. In other words, we assume that the amount of the ECM are directly proportional to the cell population without considering the detailed process of ECM secretion. The length scale constraint required in Equation (8) is as Equation (4), that is, the length scale l_σ of the cell phase must be small compared to the radius of the elementary volume.

The first bracket on the right-hand side of Equation (8) represents cell mass flux. The motion of the cells is like random walks and analogous to the process of diffusion in a macro cellular fashion. The diffusion coefficient D_{cell} can be obtained by an ensemble of the square displacements of a population of cells (Berg, 1993). It is known that cells need to attach to surrounding matrices in order to obtain sufficient traction for movement. Since autocrine matrix production may be required for the cells to locomote in a highly porous scaffold, the true diffusion coefficient of cell motion may be a function of time and space. However, for simplicity, we assume the cell diffusion coefficient in the scaffold to be a constant. It also needs to address that directed cell motion due to chemotaxis is not included in this work. Chondrocytes must respond to bona fide chemotactic attractants such as growth factors (Hidaka et al., 2006) rather than to the nutrients like glucose and oxygen. As we have not

DOI 10.1002/bit

incorporated any chemo-attractants into our model, chemotaxis should be consistently ignored in this study.

The second bracket on the right-hand side of Equation (8) accounts for the Modified Contois kinetics (Contois, 1959), which is reported to have a better fit with experimental data than the Moser and heterogeneous kinetics (Galban and Locke, 1999a). The modified Contois kinetics incorporates the effect of nutrient saturation and also a dependence on the cell amounts. Here, the coefficient K_c is the saturation coefficient, ρ_{cell} is the cell mass density, R_d is the apoptosis rate, and R_g is the maximum growth rate. In this function, cell growth rate will approach the asymptote R_g if nutrient is sufficiently supplied; if nutrient is depleted, the cell growth rate will be approximately proportion to the nutrient concentration.

We further assume that the intrinsic average mass density of the cell phase $\langle \rho_\sigma \rangle^\sigma$ is a constant. Under such a situation and in conjunction with Equation (5), the cell equation is simplified as

$$\frac{\partial}{\partial t'}\varepsilon_\sigma = D_{cell}\nabla^2\varepsilon_\sigma + \left[\frac{R_g\langle c_\beta\rangle^\beta}{K_{eq}^{-1}K_c\rho_{cell}\varepsilon_\sigma + \langle c_\beta\rangle^\beta} - R_d\right]\varepsilon_\sigma \tag{10}$$

which can be used to solve the volume fraction of the cell phase, ε_σ. Since the solid fraction of the scaffold is quit small (usually as low as 5%), it is reasonable to assume that elementary volumes comprise only cell phase and fluid phase, that is, $V = V_\beta + V_\sigma$. The volume fraction of the fluid phase thus can be determined by the following equation once the volume fraction of the cell phase is obtained

$$\varepsilon_\beta + \varepsilon_\sigma = 1 \tag{11}$$

Boundary Conditions

The scaffold is considered a square region totally submerged in a culture medium as shown in Figure 1. The condition for the nutrient concentration at the four boundaries can be treated by

$$\langle c_\beta\rangle^\beta = c_0, \quad x' = 0, \quad L'; \quad y' = 0, \quad H' \tag{12}$$

where c_0 is the nutrient concentration within the medium surrounding the scaffold. As the boundary condition for the volume fraction of cells is concerned, we assume cells cannot move out of the scaffold. Therefore, cell mass flux must equal zero on the boundaries, which can be described by the following equation with the mass density of the cell phase being assumed constant

$$(D_{cell}\nabla\varepsilon_\sigma)\cdot\boldsymbol{n} = 0 \quad x' = 0, \quad L'; \quad y' = 0, \quad H' \tag{13}$$

where $\boldsymbol{n}$ is the unit normal at the scaffold boundary.

Non-Dimensionalization

As have seen, the influential parameters in the model are numerous. It is valuable if the governing equations can be presented in a dimensionless form. By choosing adequate dimensional scales, dimensionless groups can be formed and served as interpretations of the problem. The following three scales are chosen: the inverse growth rate R_g^{-1} for time, the thickness of the scaffold H' for length, and the nutrient concentration in the ambient culture medium, c_0, for nutrient concentration, that is,

$$t = t'R_g, \quad x = x'/H', \quad y = y'/H', \quad C = \langle c_\beta\rangle^\beta/c_0 \tag{14a–d}$$

where t, x, y, and C are the dimensionless time, x- and y-coordinates and concentration. The corresponding dimensionless nutrient equation is

$$\delta\frac{\partial}{\partial t}\left[(\varepsilon_\beta + \varepsilon_\sigma K_{eq})C\right] = \nabla\cdot(D_{eff}\nabla C) - R_m\varepsilon_\sigma C \tag{15}$$

In the equation, there are three dimensionless groups

$$\delta = \frac{H^2R_g}{D_\beta}, \quad D_{eff} = \frac{\hat{D}_{eff}}{D_\beta}, \quad R_m = \frac{H^2\hat{R}_mK_{eq}}{D_\beta} \tag{16a–c}$$

The dimensionless cell equation is

$$\frac{\partial\varepsilon_\sigma}{\partial t} = \Lambda\nabla^2\varepsilon_\sigma + \left[\frac{C}{\eta\varepsilon_\sigma + C} - \lambda\right]\varepsilon_\sigma \tag{17}$$

Appearing in the equation are the three dimensionless groups

$$\Lambda = \frac{D_{cell}}{H^2R_g}, \quad \lambda = \frac{R_d}{R_g}, \quad \eta = \frac{K_c\rho_{cell}}{c_0K_{eq}} \tag{18a–c}$$

The dimensionless boundary condition for the dimensionless nutrient concentration is

$$C = 1, \quad x = 0, \quad L; \quad y = 0,\ 1 \tag{19}$$

The dimensionless boundary condition for the cell volume fraction is

$$\boldsymbol{n}\cdot\nabla\varepsilon_\sigma = 0, \quad x = 0 \quad L; \quad y = 0,\ 1 \tag{20}$$

Here L is the dimensionless width of the scaffold that is scaled by the thickness, that is, $L = L'/H'$

Solutiuon Procedure

FEMLAB (version 2.3, COMSOL) code, which utilize a finite element method, is employed to solve the dimensionless nutrient concentration C (Eq. (15)) and the volume fraction of the cell phase ε_σ (Eq. (17)) subject to the boundary conditions in Equations (19) and (20). Mesh refinement test is performed to ensure relative errors smaller than 10^{-3}. The model can be run from an initial state to a state in which the nutrient concentration is decreased to zero or the cell volume is reaching unity. A macro average cell volume fraction is define as

$$\varepsilon_{\sigma,avg} = \frac{\int_{x=0}^{L}\int_{y=0}^{1}\varepsilon_\sigma \mathrm{d}x\mathrm{d}y}{\int_{x=0}^{L}\int_{y=0}^{1}\mathrm{d}x\mathrm{d}y} \tag{21}$$

This averaged quantity obtained by averaging cell volume fractions over the entire scaffold volume can be used for convenience to compare with experimental results found in the literature, and it is also useful to condense the large number of output data.

RESULTS AND DISCUSSION

To validate the current model, simulations are conducted to compare with the experimental work of Freed et al. (1994a). Freed et al. (1994a) investigated the kinetics of chondrocyte growth in cell-polymer implants. Chondrocytes isolated from the knee joints of 2–3-week-old calves were cultivated in PGA scaffolds with various thicknesses. Porosities of the scaffolds were 92–96%. Parametric values used for the simulations are listed in Table I. The initial values of the cell volume fraction $\varepsilon_{\sigma 0}$ are calculated from the initial cell number, N_0, of Freed et al., which is listed in Table II. The seeding efficiency as reported is 60%. By assuming uniform seeding, the value of $\varepsilon_{\sigma 0}$ in each simulation case is estimated by the equation $\varepsilon_{\sigma 0} = 0.6 \cdot N_0 \cdot V_{\text{cell}}/V_{\text{scaffold}}$, where V_{scaffold} is the volume of the scaffold. Galban and Locke (1999a) found that the parameter values were sensitive to the scaffold size. They investigated a variety of parameters against the scaffold thickness and showed that the values of R_g decreased with the scaffold thickness. Here, we also adjust the cell growth rate R_g for better fits with the experimental data. The fitting values of R_g are listed in Table II. Trends and sensitivities of other parameters can be found in Galban and Locke (1999a).

The macroscopic average cell volume fractions, $\varepsilon_{\sigma,\text{avg}}$, as defined in Equation (21), are compared with the experimental data in Figure 2. The abscissa of the figure is the dimensionless time defined in Equation (14a). Notwithstanding the four groups of data have the same dimensional time spans (30 days), their dimensionless times that have been scaled by their own R_g express different dimensionless regions. Here the computations are performed with the simplified effective diffusion coefficient in Equation (7). Even this simplified formulation can give quite fair agreements with the experiments. The simulations reveal a lag-time phenomenon at the initial phase, which is arising from the Contois kinetics (Galban and Locke, 1999a). A minor deviation is observed for the 0.088 cm scaffold at the long time, for which the experiment shows the cell volume fraction can almost reach unity. The lack of fit for the smaller construct may be attributed to the breakdown of the length constraints described in Equation (4) because the length scales l_β of the cell phase may become comparable to the radius r of the elementary volume when the cell volume fraction approach unity. On the other hand, the lack of fit may also suggest that other factors, which have not yet been involved in the present model, such as biological waste, other growth moderating chemical species, and the existence of other separate domain of the ECM, may increase the sensitivity of the cell growth to variations in scaffold size (Galban and Locke, 1999a).

The influences of cell random walks are analyzed in the following. We compare the situations of uniform and non-uniform seeding with the scaffold thickness fixed at 0.307 cm. For the uniform seeding case, cell are assumed uniformly seeded in the scaffold with an initial cell volume fraction $\varepsilon_{\sigma 0} = 0.00548$. For the non-uniform case, cells are assumed to be concentrated in the circular regions as indicated in Figure 3, the area of which is a tenth of the whole scaffold. Outside of the seeded region, the cell volume fraction is initially set zero; inside of the seeded region, the initial cell volume fraction is set to be $\varepsilon_{\sigma 0} = 0.0548$, ten times of the uniform seeding counterpart, so that for the two cases, the initial cell numbers in the whole scaffold are the same. All other parametric values are associated with the case of 0.307 cm scaffold as listed in Tables I and II. The corresponding dimensionless parametric values are $\delta = 0.15$, $R_m = 9.4$, $\Lambda = 1.2 \times 10^{-4}$, $\lambda = 2.1 \times 10^{-2}$, and $\eta = 620$. Comparison of the macro average cell volume fraction is displayed in Figure 4. As shown, concentrate seeding results in a large initial lag in growth, and, therefore, the overall cell growth is less than the uniform seeding case.

Figures 5 and 6 show the contours of the nutrient and cell volume fraction at $t = 50$ (real time 36 days) for the uniform

Table I. List of parameters.

Cellular parameters
Specific cell volume $V_{\text{cell}} = 549\ \mu\text{m}^3$/cell Bush and Hall (2001)
Specific cell weight $M_{\text{cell}} = 10^{-10}$ g/cell Martin et al. (2001)
Cell density $\rho_{\text{cell}} = M_{\text{cell}}/V_{\text{cell}} = 0.182$ g/cm^3
Substrate parameters
Glucose concentration in the surrounding medium $c_0 = 4.5 \times 10^{-3}$ g/cm^3 Freed et al. (1994a)
Glucose diffusion coefficient in the cell phase $D_\sigma = 1.0 \times 10^{-6}$ cm^2/s Galban and Locke (1999a)
Glucose diffusion coefficient in the fluid phase $D_\beta = 1.0 \times 10^{-5}$ cm^2/s Galban and Locke (1999a)
Equilibrium coefficient $K_{\text{eq}} = 0.1$ Galban and Locke (1999a)
Metabolic parameters
Maximum consumption rate of glucose $\hat{R}_m = 3.0 \times 10^{-2}/\text{s}$ Galban and Locke (1999a)
Growth and migration parameters
Maximum cell growth rate $R_g = 1.6\text{–}4.5 \times 10^{-5}\text{s}^{-1}$
Cell dying rate $R_d = 3.3 \times 10^{-7}$ s^{-1} (cells are assumed to live 30 days on average)
Contois saturation coefficient $K_c = 1.54$ Galban and Locke (1999a)
Diffusion coefficient of cellular random motion $D_{\text{cell}} = 1.7 \times 10^{-10}$ cm^2/s Barocas et al. (1995)

DOI 10.1002/bit

Table II. Initial values of ε_σ and physical values of R_g used in the simulations

Scaffold thickness (cm)	Initial cell number N_0 ($\times 10^6$cells) Freed et al. (1994a)	$\varepsilon_{\sigma 0}$ (Seeded initially) zero-time	R_g ($\times 10^{-5}$/s)
0.088	2	0.00953	4.2
0.116	2	0.00726	3.8
0.168	2	0.005	2.2
0.307	4	0.00548	1.6

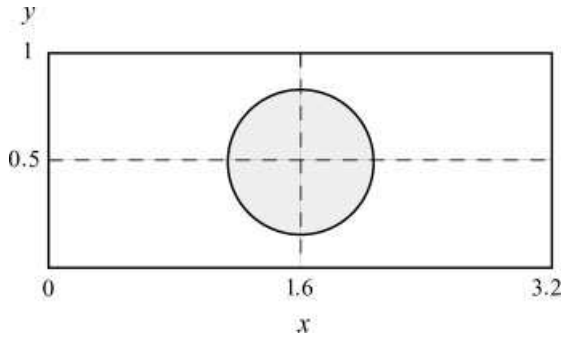

Figure 3. Schematic of non-uniform seeding. Cells are assumed to be seeded only in the circular region at the center with the initial cell volume fraction $\varepsilon_{\sigma 0} = 0.0548$. The seeding circle is one-tenth the area of the whole construct.

and concentrate seeding, respectively. The nutrient distributions are similar in the two situations as shown in Figures 5a and 6a. Due to the fact that nutrients are diffused from the scaffold periphery into the central region, nutrients in both the cases are of maximum value around the scaffold boundaries and of minimum at the center. Figure 5b shows that the cell distribution of the uniform seeding case has a similar pattern to the nutrient distribution because of the transport constraint of the nutrients. However, the cell distribution of the concentrate seeding has quite different contour pattern. Beginning with a round colony, cells grow and spread from the seeding region toward the scaffold periphery. The contours of the cell volume fraction (i.e., the cell number density) at initial phase are concentric circles (not shown) when the cell colony has not yet reached the scaffold boundary. At this stage, the cell number density is highest at the center of the seeding region. As the cultivation carries on, cell distributions evolve and become to locate quite differently. After cells have reached the scaffold top and bottom (Fig. 6b); the cell number density becomes largest at both the top and bottom of the scaffold because of the sufficient nutrient supply there, while the cell number density is still small at both the left and right sides because cells have not yet move to there. The cell distributions in the middle x- and y-diections, respectively are shown in Figure 7 for the uniform seeding case. The local minimum at the center is obvious. The non-uniform counterparts are shown in Figure 8. It is seen the central region is of local maximum cell density in the x-direction while local minimum in the y-direction.

The effects of cell random walks are further investigated. As defined in Equation (18a), the dimensionless parameter that is directly related to the cellular motion is Λ, which account for the ratio of random walks to cell growth rate. Shown in Figure 9 is the macro average cell volume fraction against dimensionless time for various Λ values. It is found random walks have a unitary effect, which increases the cell

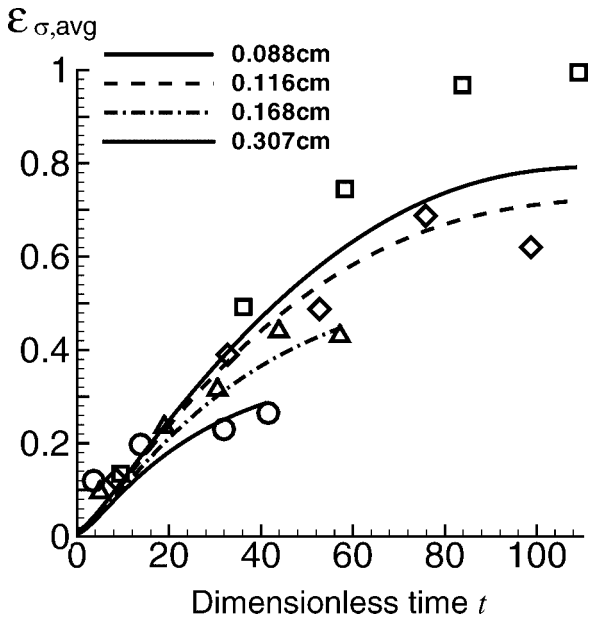

Figure 2. Comparison of the present model and experimental data of Freed et al. (1994a). The dimensionless time is scaled with R_g^{-1} respectively for different scaffold.

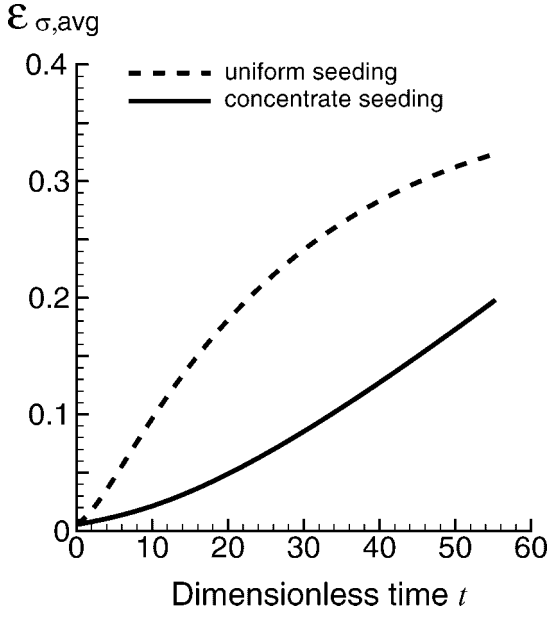

Figure 4. Comparison of the time evolution of the macro average cell volume fraction for the uniform seeding (dashed line) and non-uniform seeding (solid line). Dimensionless parameters are $\delta = 0.15$, $R_m = 9.4$, $\Lambda = 1.2 \times 10^{-4}$, $\lambda = 2.1 \times 10^{-2}$, and $\eta = 620$.

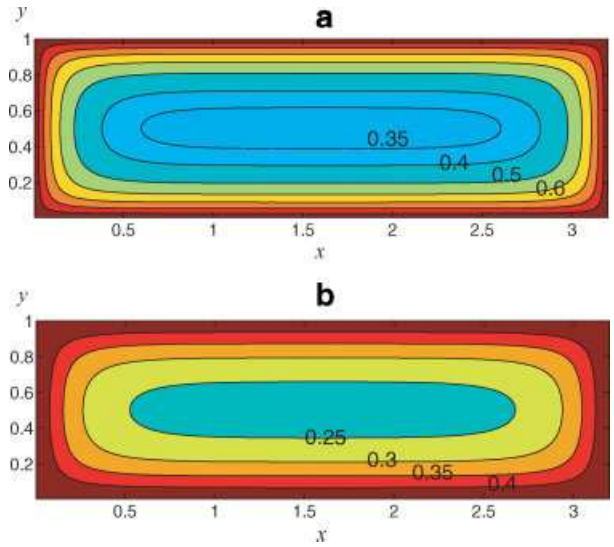

Figure 5. Contours of nutrient (**a**) and contours of cell volume fraction (**b**) at dimensionless time $t = 50$ (real time 36 days) for the uniform seeding case. Dimensionless parametric values are the same as those used in Figure 4. The contour values of the nutrient range from 0.35 to 1 with the maximum at the construct periphery. The contour values of cell volume fraction range from about 0.25 to 0.45 also with the maximum at the construct periphery. [Color figure can be seen in the online version of this article, available at www.interscience.wiley.com.]

growth rate. By the diffusion process of cell random walks, cells are able to spread more widely over the scaffold, preventing crowding in a local area to compete for nutrients, therefore, cell growth increases effectively with increasing Λ.

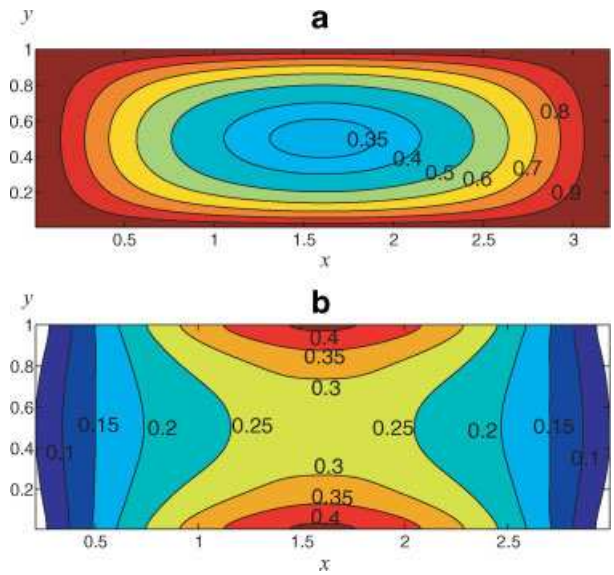

Figure 6. Contours of nutrient (**a**) and contours of cell volume fraction (**b**) at dimensionless time $t = 50$ (real time 36 days) for the non-uniform seeding case. Dimensionless parametric values are the same as those used in Figure 4. The contour values of the nutrient range from 0.35 to 1 with the maximum at the construct periphery. The contour values of cell volume fraction range from 0 to about 0.4 with the maximum at both the construct top and bottom and minimum at both the left- and right-hand sides. [Color figure can be seen in the online version of this article, available at www.interscience.wiley.com.]

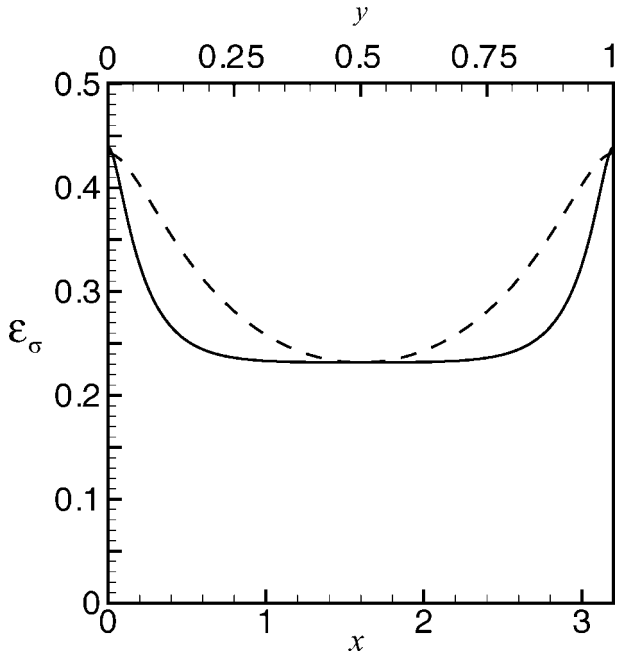

Figure 7. Distributions of cell volume fraction along $y = 0.5$, the middle x-direction (solid line), and along $x = 1.6$, the middle y-direction (dashed line) of the cell-scaffold construct for the case of uniform seeding.

CONCLUSIONS

In this article, a mathematical model for cell generation and diffusion is developed to investigate chondrogenesis and glucose consumption in a cell-polymer construct. Comparisons with experimental data in the literature show that the model can work well provided the scaffold is not too thin. The

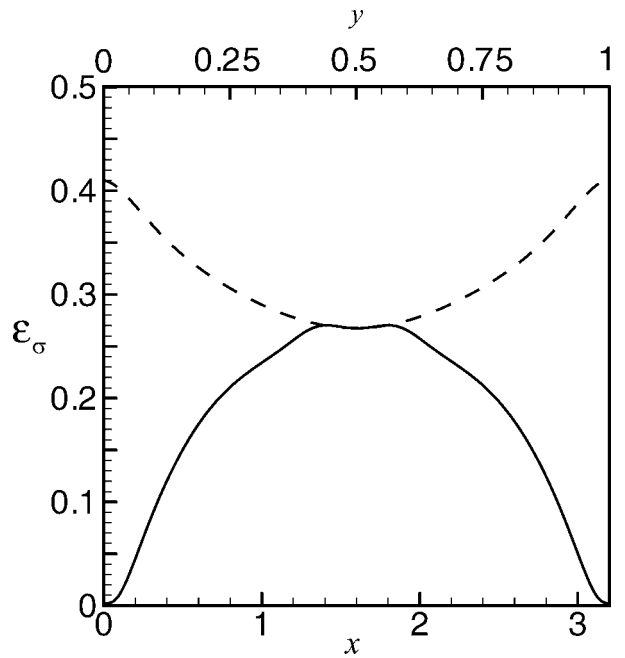

Figure 8. Distributions of cell volume fraction along $y = 0.5$, the middle x-direction (solid line) and along $x = 1.6$, the middle y-direction (dashed line) of the cell-scaffold construct for the case of non-uniform seeding.

DOI 10.1002/bit

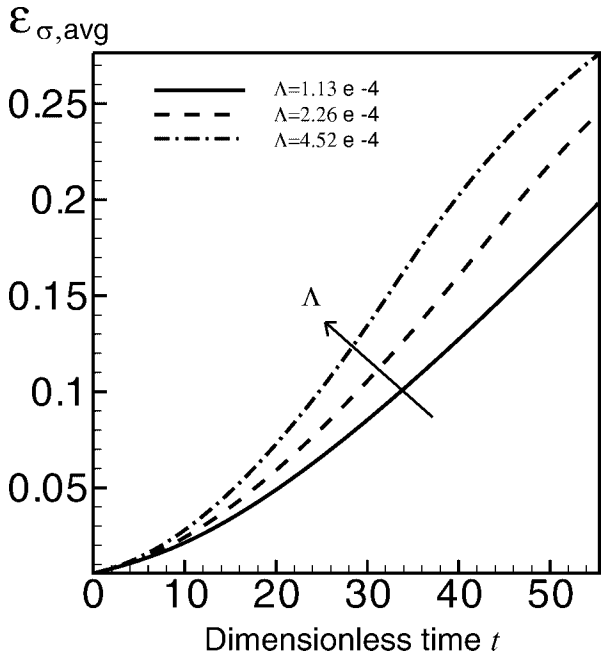

Figure 9. Time evolution of the macro average cell volume fraction for the non-uniform seeding case and different values of Λ.

deviation between the simulation and experiment for the thin-scaffold case may be due to the breakdown of the length scale constraints described in Equation (4) as the length scales l_β of the cell phase may become comparable to the radius r of the elementary volume once the cell volume fraction approach unity, which eventually violet the length constraints in the method of volume average. The other possible reasons for the lack of fit may be from other factors we have not involved in the model, such as biological waste, other growth moderating chemical species, and the existence of other separate domain such as the ECM. They may all increase the sensitivity of the cell growth to the variations in scaffold size (Galban and Locke, 1999a).

The cell random motion is incorporated into the model by the cell diffusion term in the cell balance equation. Results show that random walks help spread cells more uniformly in space, which in turn prevents cells to compete for nutrients around a local area. As a result, the overall cell growth rate will be higher than the case without random walks. By incorporating cell motility into the present model, we investigate the effects of non-uniform seeding, considering parts of the scaffold have not been seeded. It is shown that uniform seeding is likely to be a better strategy than the non-uniform, concentrate seeding for increasing cell growth rates. Non-uniform, concentrate seeding implies higher initial cell densities at a local area and results in competition for nutrients, which in conjunction with the nutrient transport limits, would reduce the overall cell growth. According to our investigations, scaffold materials and architectures should be designed to favor random walks for increasing cell growth rates. Finally, it needs to address that chemotaxis effects have not been involved into the present model. To investigate the chemotactic effects, distributions of chemotactic factors, such as basic fibroblast growth factor (Hidaka et al., 2006), must be incorporated into the model. Since, we have considered only the major nutritious species (glucose) in the work, it should be consistent to remove chemotaxis in the model. To our knowledge, modeling chemotaxis for in vitro generation of chondrocytes has not been investigated thoroughly, and shall merit further research efforts.

NOMENCLATURE

Roman Letters

c_0	nutrient concentration in the surrounding medium [g/cm^3]
c_β	nutrient concentration in the β-phase [g/cm^3]
c_σ	nutrient concentration in the σ-phase [g/cm^3]$\langle c_\beta \rangle^\beta$
$\langle c_\beta \rangle^\beta$	intrinsic average concentration of nutrient in the β-phase [g/cm^3]
$\langle c_\sigma \rangle^\sigma$	intrinsic average concentration of nutrient in the σ-phase [g/cm^3]
C	$\langle c_\beta \rangle^\beta / c_0$, dimensionless intrinsic average nutrient concentration in the β-phase
D_{cell}	diffusion coefficient for cellular random motion [cm^2/s]
D_β	diffusivity for nutrient in the β-phase [cm^2/s]
D_σ	diffusivity for nutrient in the σ-phase [cm^2/s]
$\hat{\mathbf{D}}_{\text{eff}}$	overall effective diffusion tensor for the equilibrium model [cm^2/s]
$\hat{D}_{\text{eff}}$	overall effective diffusivity for the equilibrium model [cm^2/s]
D_{eff}	$\hat{D}_{\text{eff}}/D_\beta$, dimensionless overall effective diffusivity defined in Equation (16b)
$\mathbf{D}^\beta_{\text{eff}}$	effective diffusion tensor in the β-phase [cm^2/s]
$\mathbf{D}^\sigma_{\text{eff}}$	effective diffusion tensor in the σ-phase [cm^2/s]
H'	thickness of the scaffold [cm]
$\boldsymbol{I}$	unit tensor
K_{c}	Contois saturation coefficient
K_{eq}	Equilibrium coefficient
L'	width of the scaffold [cm]
L	L'/H', dimensionless width of the scaffold
l_β	characteristic length of the β-phase [cm]
l_σ	characteristic length of the σ-phase [cm]
M_{cell}	specific cell mass [g/cell]
N_0	initial cell number seeded in scaffold [cells]
$\boldsymbol{n}$	unit out normal vector at the boundary of cell-scaffold construct
R_{d}	cell dying rate [per s]
R_{g}	maximum cell growth rate [per s]
$\hat{R}_{\text{m}}$	metabolic rate [per s]
R_{m}	$\hat{R}_{\text{m}} H^2 K_{\text{eq}}/D_\beta$, dimensionless parameter defined in Equation (16c)
t	$t' R_{\text{g}}$, dimensionless time
t'	time [s]
V	elementary volume [cm^3]
V_{cell}	specific cell volume [μm^3/cell]
V_β	volume of the β-phase in the elementary volume [cm^3]
V_σ	volume of the σ-phase in the elementary volume [cm^3]
r	characteristic radius of the elementary volume [cm]
x	x'/H', dimensionless horizontal coordinate
x'	horizontal coordinate [cm]
y	y'/H', dimensionless vertical coordinate
y'	vertical coordinate [cm]

Greek Letters

δ	$H^2 R_{\text{g}}/D_\beta$, dimensionless parameter defined in Equation (16a)
ε_β	V_β/V, volume fraction of the β-phase
ε_σ	V_σ/V, volume fraction of the σ-phase
$\varepsilon_{\sigma 0}$	initial volume fraction of the σ-phase at $t = 0$
$\varepsilon_{\sigma,\text{avg}}$	macroscopic average of cell volume fraction over the entire cell-scaffold construct

η	$K_c\rho_{cell}/(c_0K_{eq})$, dimensionless parameter defined in Equation (18c)
λ	R_d/R_g, dimensionless parameter defined in Equation (18b)
Λ	$D_{cell}/(H^2R_g)$, dimensionless parameter defined in Equation (18a)
ρ_{cell}	M_{cell}/V_{cell} specific cell density [g/cm^3]
ρ_σ	mass density of the σ-phase [g/cm^3]
$\langle c_\sigma \rangle^\sigma$	intrinsic average mass density of the σ-phase [g/cm^3]

This work is supported by the grant from the National Science Council of Taiwan, which is greatly acknowledged.

References

Barocas VH, Moon AG, Tranquillo RT. 1995. The fibroblast-populated collagen microsphere assay of cell traction force-part2: Measurement of the cell traction parameter. J Biomech Eng 117:161–170.

Berg HC. 1993. Random walks in Biology. Princeton: Princeton University Press. Chap 1.

Britton NF. 2002. Essential mathematical biology. London: Springer-Verlag. Chap 5.

Bush PG, Hall AC. 2001. Regulatory volume decrease (RVD) by isolated and in situ bovine articular chondrocytes. J Cell Physiology 187:304–314.

Carbonell RG, Whitaker S. 1984. Heat and mass transport in porous media. In: Bear J, Corapcioglu MY, editors. Machanics of fluids in porous media. Brussels: Martinus Nijhoff.

Chang H-C. 1983. Effective diffusion and conduction in two-phase media: A unified approach. AICHE J 29:846–853.

Chang C, Lauffenburger DA, Morales TI. 2003. Motile chondrocytes from newborn calf: Migration properties and synthesis of collagen II. Osteoarthritis Cartilage 11:603–612.

Contois DE. 1959. Kinetics of bacterial growth: Relationship between population density and specific growth rate of continuous cultures. J Gen Microbil 21:40–50.

Freed LE, Vunjak-Novakovic G, Marquis JC, Langer R. 1994a. Kinetics of chondrocyte growth in cell-polymer implants. Biotechnol Bioeng 43:597–604.

Freed LE, Marquis JC, Vunjak-Novakovic G, Emmanual J, Langer R. 1994b. Composition of cell-polmer cartilage implants. Biotechnol Bioeng 43:605–614.

Frenkel SR, Clancy RM, Ricci JL, Di Cesare PE, Rediske JJ, Abramson SB. 1996. Effect of nitric oxide on chondrocyte migration, adhesion and cytoskeletal assembly. Arthritis Rheum 39:1905–1912.

Galban CJ, Locke BR. 1999a. Analysis of cell growth kinetics and substrate diffusion in a polymer scaffold. Biotechnol Bioeng 65:121–132.

Galban CJ, Locke BR. 1999b. Effects of spatial variation of cells and nutrient and product concentrations coupled with product inhibition on cell growth in a polymer scaffold. Biotechnol Bioeng 64:633–643.

Griffith LG, Naughton G. 2002. Tissue engineering—Current challenges and expanding opportunities. Science 295:1009–1014.

Hamilton DW, Riehle Mo, Monaghan W, Curtis ASG. 2005. Articular chondrocyte passage number: Influence on adhesion, migration, cytoskeletal organization and phenotype in response to nano- and micro-metric topograph. Cell Biol Int 29:408–421.

Hidaka C, Cheng C, Alexandre D, Bhargava M, Torzilli PA. 2006. Maturational differences in superficial and deep zone articular chondrocytes. Cell Tissue Res 323:127–135.

Hillesdon AJ, Pedley TJ, Kessler JO. 1995. The development of concentration gradients in a suspension of chemotactic bacteria. Bull Math Biol 57:299–344.

Langer R, Vacanti P. 1993. Tissue engineering. Science 260:920–925.

Lewis MC, Macarthur BD, Malda J, Pettet G, Please CP. 2005. Heterogeneous proliferation within engineered cartilaginous tissue: The role of oxygen tension. Biotecnnol Bioeng 91:607–615.

Malda J, Woodfield TBF, van der Vloodt F, Wilson C, Martens DE, Tramper J, van Blitterswijk CA, Riesle J. 2005. The effect of PEGT/PBT scaffold architecture on the composition of tissue engineered cartilage. Biomaterials 26:63–72.

Martin I, Suetterlin R, Baschong W, Heberer M, Vunjak-Novakovic G, Freed LE. 2001. Enhanced cartilage tissue engineering by sequential exposure of chondrocytes to FGF-2 during 2D expansion and BMP-2 during 3D cultivation. J Cell Biochem 83:121–128.

Obradovic B, Carrier RL, Vunjak-Novakovic G, Freed LE. 1999. Gas exchange is essential for bioreactor cultivation of tissue engineered cartilage. Biotechnol Bioeng 63:197–205.

Obradovic B, Meldon JH, Freed LE, Vunjak-Novakovic G. 2000. Glycosaminoglycan deposition in engineered cartilage: Experiments and mathematical model. AIChE J 46:1860–1871.

Ochoa JA, Stroeve P, Whitaker S. 1986. Diffusion and reaction in cellular media. Chen Eng Sci 41:2999–3013.

Pachence JM, Kohn J. 2000. Biodegradable polymers. In: Lanza RP, Langer R, Vacanti J, editors. Principles of tissue engineering. San Diego: Academic Press. p 263–277.

Pazzano D, Mercier KA, Moran JM, Fong SS, DiBiasio DD, Rulfs JX, Kohles SS, Bonassar LJ. 2000. Comparison of Chondrogensis in static and perfused bioreactor culture. Biotechnol Prog 16:893–896.

Peppas NA, Langer R. 1994. New challenges in biomaterials. Science 263:1715–1720.

Wood BD, Quintard M, Whitaker S. 2002. Calculation of effective diffusivities for biofilms and tissues. Biotechnol Bioeng 77:495–516.

DOI 10.1002/bit